The Melting Line, the Crystallization Line, and the Equilibrium Melting Temperature of Isotactic Polystyrene

M. Al-Hussein* and G. Strobl

Fakultät für Physik, Albert-Ludwigs-Universität, Hermann-Herder-Str. 3 79104 Freiburg, Germany

Received July 30, 2001; Revised Manuscript Received November 24, 2001

ABSTRACT: It is known that the determination of the equilibrium melting temperatures of polymers which show recrystallization during heating is a difficult problem. This is mainly due to the difficulty encountered in determining the melting temperature of the initial lamellae which exist before recrystallization takes place. We are reporting here the results of a study investigating this problem for a representative polymer, namely isotactic polystyrene. Both the crystallization line and the Gibbs−Thomson melting line were constructed on the basis of time- and temperature-dependent SAXS measurements, respectively. When the two lines are plotted on the same graph, they intersect each other at a finite crystal thickness and at temperature of about 243 °C. This temperature is very close to the commonly reported values of the equilibrium melting temperature of isotactic polystyrene obtained using the Hoffman−Weeks extrapolative method, namely 242 °C. However, the value obtained from the intercept of the Gibbs−Thomson melting line is found to lie in the range of 289 ± 5 °C. This new, higher value of the equilibrium melting temperature of isotactic polystyrene might justify the high melting temperatures found for some isotactic polystyrene samples, which were as high as 255 °C for samples with a shish kebab morphology. Finally, DSC curves were recorded for samples crystallized at different crystallization temperatures in order to compare the Gibbs−Thomson melting line obtained by the SAXS measurements and that obtained by the DSC curves. The result of such comparison showed a good agreement.

1. Introduction

The equilibrium melting temperature of a polymer, T_f^∞, is the thermodynamic quantity which defines the melting temperature of an equilibrium crystal, i.e., of infinite size, of that polymer. The difference between T_f^∞ and the crystallization temperature defines the undercooling which is proportional to the thermodynamic driving force for crystallization. In most of the crystallization theories,[1,2] a prior knowledge of T_f^∞ is necessary for the derivation of other parameters, such as the nucleation constant or the basal surface free energy of a crystal. A direct measurement of T_f^∞ is not available, and it can only be determined using extrapolation procedures. This is due the fact that polymer equilibrium crystals cannot be prepared experimentally as polymers crystallize only partially.[3] The two most commonly used procedures in this course are the Gibbs−Thomson (G−T)[4] and the Hoffman−Weeks (H−W)[5] methods. The G−T method is based upon a thermodynamic relationship describing the melting temperature depression of nanosize crystals below that of a macroscopic crystal. According to this relationship, the melting temperature depression $T_f^\infty - T_f$ is proportional to the ratio of the crystal basal surface free energy to the lamellar thickness, d_c. Consequently, if the melting temperature is plotted as a function of the reciprocal of the crystal thickness, the intercept of the extrapolation of a linear regression of that plot gives T_f^∞. The H−W method is based upon both the G−T equation and the surface nucleation theory. It has been extensively used by many workers to determine T_f^∞ for many polymers. The reason behind this popularity is its straightforward use as only one readily measurable quantity is needed to determine T_f^∞, namely the melting temperature, T_f, of the crystallites formed at T_c. In its common form, it encompasses the extrapolation of a linear fit of the T_f vs T_c plot to the line $T_f = T_c$, and the intercept value is taken as T_f^∞.

Over the past few years, we have studied the melting behavior, subsequent to an isothermal crystallization, of several semicrystalline polymers through systematic temperature-dependent SAXS measurements. This included syndiotactic polypropylene, different syndiotactic poly(propene-*co*-octene)s,[6,7] poly(ethylene-*co*-octene)s,[8] poly(caprolactone),[8] isotactic polypropylene,[9] and poly(1-butene).[10] Through monitoring the changes in morphological parameters such as the crystal thickness and the long period during heating to the melt, two behaviors were observed. First, a simple melting, whereby melting started immediately at temperatures just above the crystallization temperature and then extended up to T_f without any detectable change in the crystal thickness. The second behavior was observed when the sample underwent a recrystallization after melting during the heating scan. Here, the crystal thickness kept constant up to the melting temperature of the initial lamellae, and then recrystallization took place and resulted in higher values of the crystal thickness associated with the recrystallized lamellae which then melted at higher temperatures. These studies allowed the opportunity to study the relationships between T_c, T_f, and d_c for the same lamellae. Plots of both T_c and T_f as functions of d_c^{-1} on the same graph always yielded two different lines: a crystallization line, T_c vs d_c^{-1}, in addition to the G−T melting line, T_f vs d_c^{-1}. An important result of these representations was that the melting and crystallization lines intersect each other at a finite d_c. This contradicts the basic assumption of the H−W extrapolation method, where the intersection of these two lines should occur for the infinite equilibrium crystal, i.e., at $d_c^{-1} = 0$. The difference between the temperature at the intersection and that at $d_c^{-1} = 0$, which represents the true value of T_f^∞, was as many as

10.1021/ma011345k CCC: $22.00
Published on Web 01/22/2002

20 °C in some cases.[8] The values of the temperatures at which the two lines intersect each other are always comparable to the reported values of T_f^∞ obtained by the H−W extrapolative method. This casts considerable doubts on the correctness of many of the reported values of T_f^∞ for different polymers. It is worth mentioning here that the H−W relation was shown by Marand[11] to be incapable of determining T_f^∞ accurately, and instead he proposed a nonlinear approach which takes account of a constant thermodynamics driving force. However, Marand's nonlinear approach is founded upon an assumed lamellar growth model, namely the surface nucleation model. Despite the fact that this model has been used by many workers for a long time, the past few years have witnessed the reporting of an increasing amount of experimental evidence which indicates the inadequacy of this model. In fact, doubts in its validity arise not only from our SAXS results but also in view of the early stage morphology of crystallizing PE in Kanig's TEM images[12] which greatly differs from continuous lamellae, IR spectroscopic observations of chain conformations typical for the hexagonal phase at the crystallization onset of PE,[13] the time difference in the evolution of V_V- and V_H-light scattering at the early stages of iPP-crystallization,[14] direct AFM-real time observations of growing PE-lamellae, which show variations in the individual growth rate between different lamellae and also for a given crystal as a function of time and structured growth faces which are far away from being flat,[15,16] and oriented crystal growth in magnetic fields.[17] This cites only a few of several new experimental findings (for a detailed discussion compare ref 18).

The G−T melting line can be determined by the temperature-dependent SAXS measurements as they provide the opportunity to record the melting temperature and the crystal thickness simultaneously. In contrast to the H−W plot which relies on a preassumed lamellar growth model, the determination of T_f^∞ by a linear extrapolation of the G−T line is based on equilibrium thermodynamics. The construction of this line is a straightforward procedure for samples that show a simple melting. For polymers that show a recrystallization during heating, one has to make sure that the measured crystallization and melting temperatures are of the same lamellae. It is known that the recrystallization phenomenon is a heating rate dependent. If the heating rate is increased to a certain value, recrystallization can sometimes be suppressed and a simple melting is observed again. This might seem as the optimum solution to determine T_f of the initial lamellae; however, one has to be aware that superheating effects could be introduced when high heating rates are used.

In this paper, we have tackled the problem of determining the equilibrium melting temperature for isotactic polystyrene which can be considered as a representative polymer of those polymers which show recrystallization during the heating scan. It turned out that even when recrystallization takes place, it is possible to construct the melting line and the crystallization line from the time- and temperature-dependent SAXS measurements. A comparison was also drawn between the melting line obtained from the SAXS measurements and that obtained using normal DSC measurements.

2. Experimental Section

2.1. Sample Characteristics and Preparation. Isotactic polystyrene (iPS) with weight-average molecular weight of 400 000 purchased from Scientific Polymer Products Inc. was used in this study. We used the compound as received, without trying to remove a possibly included atactic component. The tacticty value given by the producer was 90%. Cold crystallized samples were prepared by melting the sample first at 250 °C for 20 min under vacuum without pressure and then quenching it into an ice/water mixture. Then the sample was transferred as quickly as possible to the temperature-controlled cell of the SAXS camera which was preset at a desired crystallization temperature. When the samples completed their crystallization, they were subsequently heated to the melt in a stepwise manner.

2.2. SAXS Measurements. 2.2.1. Instrumentation. The SAXS curves were recorded using an evacuated compact Kratky camera attached to a conventional Cu X-ray tube. The scattering curves were registered using a position-sensitive detector within a few minutes counting time. The SAXS curves were desmeared using an algorithm developed in our group.[19] It works with finite, trapezoidal slit profiles and determines also the (larger) data range required for obtaining pinhole scattering intensities within a certain desired small angle range.

2.2.2. Data Analysis. Being aware of the existence of an interphase layer at the basal crystal surface, one first has to ask about the definition of the crystal thickness d_c that is used in the Gibbs−Thomson relation. The natural choice is the integral thickness, i.e., the one which would produce for a crystal with sharp boundaries the identical density increase per unit area. This is a well-defined quantity and the properties of the surface region through the interphase layer then can be included in a global manner in the surface free energy. Therefore, one has to look for means to derive this quantity from the SAXS curves, together with the Porod coefficient.

$$P = \frac{1}{8\pi^3} O_{ac}(\rho_e^c - \rho_e^a)^2 \tag{1}$$

P is determined by the difference in density $(\rho_e^c - \rho_e^a)$ between the crystal core and the melt and by the interface area per unit volume O_{ac}. There are two different ways to proceed, the first one employing the one-dimensional correlation function

$$k(z) = \frac{1}{r_e^2(2\pi)^3}\int_0^\infty \cos(qz)4\pi q^2\Sigma(q)\,dq \tag{2}$$

where q is the scattering vector, $q = 4\pi \sin\theta_B/\lambda$, θ_B denotes the Bragg angle, $\Sigma(q)$ is the differential cross section per unit volume, and r_e is the classical electron radius. Here we can use the concept of an ideal two-phase system corresponding to the real system. This ideal system is just composed of crystallites having the integral thickness, and the latter follows from a well-known, widely used graphical procedure.[3] Applying this procedure implies that any existing transition layer will be disregarded. This is preferable, because it is principally difficult to derive from SAXS curves structural features with lengths around 1 nm; they are not well resolved from microscopic structure fluctuations.

The second way, mostly employed in this work, makes use of the second derivative, $k''(z)$, of the correlation function. As was shown by Ruland,[20] for a two-phase layered system, the second derivative of the correlation function can be expressed as a series of the distributions of the distances between the interfaces:

$$k''(z) = \frac{O_{ac}}{2}(\rho_e^c - \rho_e^a)^2[h_a(z) + h_c(z) - 2h_{ac}(z) + h_{aca}(z) + h_{cac}(z) \ldots] \tag{3}$$

h_a and h_c are the distributions of the thickness of the amorphous and the crystalline layers, respectively, and h_{ac} is

their sum which is identical to the long period. Correspondingly, $k''(z)$ is often also addressed as interface distance distribution function (IDF). Rather than carrying out the 2-fold differentiation $k''(z)$, it can also be directly calculated using the equation

$$k''(z) = \frac{2}{r_e^2(2\pi)^2}\int_0^\infty [\lim_{q\to\infty} q^4\Sigma(q) - q^4\Sigma(q)] \cos(qz)\, dq \quad (4)$$

The limiting value entering into this equation is given by the Porod coefficient from

$$\lim_{q\to\infty} \Sigma(q) = r_e^2 \frac{P}{(q/2\pi)^4} \quad (5)$$

By a controlled modification of eq 4, the IDF can be calculated in a manner which again disregards the transition layer. We apply an iterative procedure to subtract the diffuse fluid scattering and simultaneously determine the Porod coefficient, using the condition that the IDF, calculated by eq 4, should vanish for $q = 0$, since this follows from eq 3. In the calculation of the integral we multiply the integrand by a Gaussian damping factor $\exp(-\sigma^2q^2/2)$. By choosing a width σ of, for example, 1 nm, we remove from the evaluation all structural features on similar and smaller length scales. We always adjust σ to the system under study. For thin lamellae (4−5 nm) we go down to 0.5 nm; for thick lamellae (10 nm and larger) we go up to 1.5 nm. Comparison of the results derived from the 1d correlation function and the IDF, which we carried out repeatedly, showed in general a good agreement.

In the evaluation the focus is only on the location of the peak maximum. One cannot derive from the peak shape valuable information, since it is affected not only by a possible thickness distribution and a possible transition layer but also by the curvature of lamellae and the width of the damping function.

2.2.3. DSC Measurements. A Perkin-Elmer DSC-7 was used to record the melting curves of isothermally crystallized samples from the two polymers. Temperature calibration was performed using standard indium and zinc samples. Cold crystallized iPS samples were prepared by melting at 250 °C for 20 min followed by quenching to 0 °C at a cooling rate of −200 °C/min to produce a totally amorphous sample. Then it was heated rapidly to a desired T_c at a heating rate of 200 °C/min. After isothermal crystallization, the samples were heated immediately to the melt. When deriving DSC crystallinities, we referred to an ideal heat of fusion of $\Delta h_{id} = 86.3$ J g^{-1}.[21]

3. Results and Discussion

Figure 1 shows as one example the changes in the IDF during heating after an isothermal crystallization at 155 °C. One observes one peak, which decreases in amplitude on heating and shows a continuous shift to higher z values, setting in at temperatures around 90 °C. Principally, according to eq 3, the IDF includes contributions from both the crystallites and the amorphous intracrystalline regions. One may wonder at first why only one and not two peaks at locations corresponding to the thicknesses of both the lamellar crystallites and the amorphous layers show up. Electron microscopic images, and many have been obtained, for example, by Petermann and co-workers,[22,23] give the answer. iPS contains after an isothermal crystallization laterally extended crystallites of uniform thickness; their distance, i.e., the long spacing, however, varies. The IDF reflects this situation and shows only the peak associated with the crystallites. Support comes also from the DSC crystallinity amounting to 0.30 ± 0.02. It agrees with the SAXS crystallinity $d_c/L = 0.31 \pm 0.01$

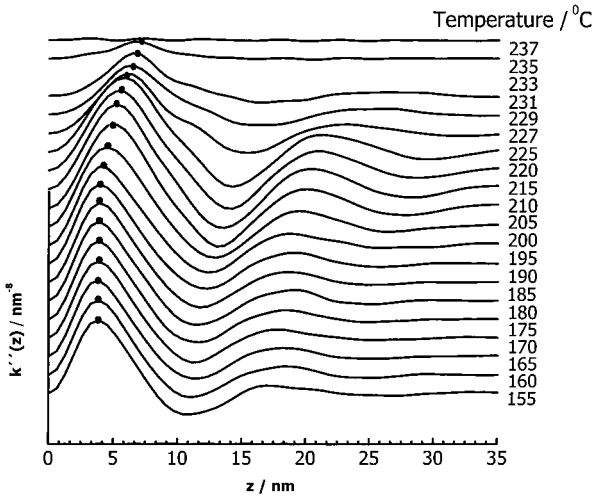

Figure 1. iPS isothermally crystallized at 155 °C. IDFs derived from the SAXS curves measured during heating to the melt.

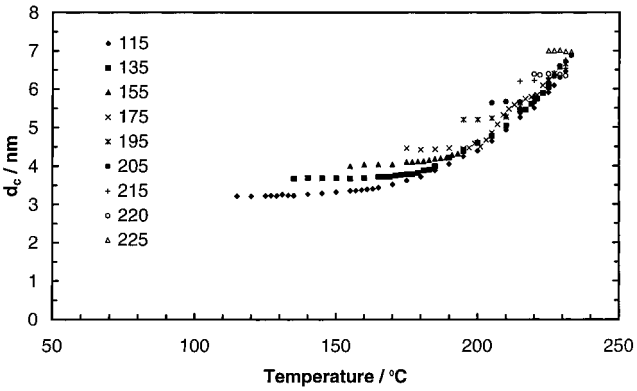

Figure 2. Variation of the crystalline thickness during subsequent heating to the melt of samples isothermally cold crystallized at the indicated crystallization temperatures.

(the long spacing L being taken from the location of the minimum in the IDF).

Figure 2 shows the changes of the crystalline thickness, extracted from the temperature-dependent SAXS measurements like the one in Figure 1 during heatings to the melt of samples isothermally cold crystallized at different temperatures. The results can be divided into three different ranges according to the crystallization temperature. First, for crystallization temperatures higher than 220 °C, no detectable change in the crystal thickness can be seen up to the final melting. Second, for crystallization temperatures between 175 and 220 °C, the crystal thickness kept constant first up to a certain temperature and then it increased gradually at increasing temperature. The third range includes samples crystallized at temperatures lower than 175 °C. Here, the gradual increase in the crystal thickness started at earlier stages of the heating scan. This difference in behavior for different crystallization temperatures might be due to the occurrence of one or more of the following phenomena during the heating scan. First, a melting−recrystallization process may take place, and this results in thicker crystallites. Second, parts of the chains that were excluded first from crystallization at the initial crystallization temperature may crystallize at higher temperatures. This might also be accompanied by a perfectioning process of the initial crystallites. The latter two phenomena apparently showed up in the third

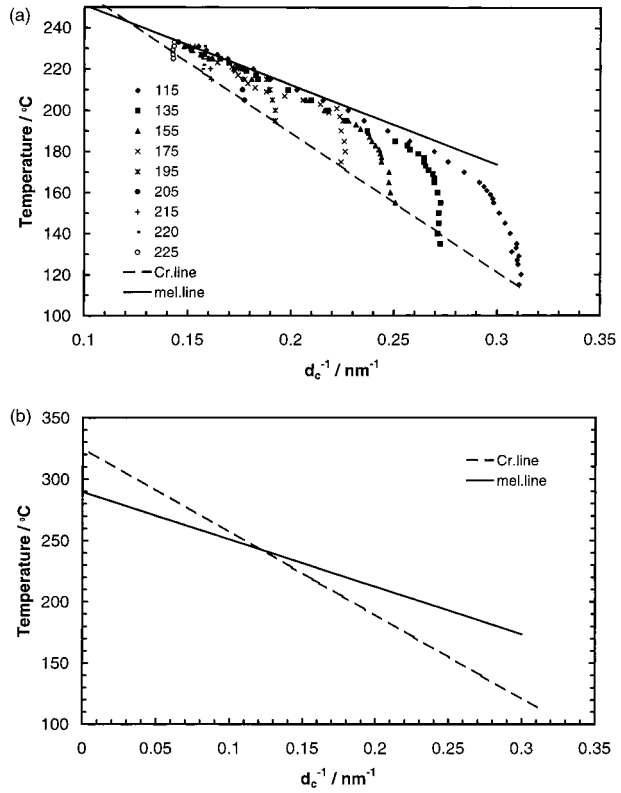

Figure 3. Variation of d_c^{-1} during heating scans subsequent to isothermal crystallizations at the indicated crystallization temperatures (a). Extrapolations of the crystallization line and the melting line to $d_c^{-1} = 0$ (b).

range. It is known that crystallites of poor quality are produced for samples crystallized at high undercooling. Upon heating such samples, they undergo further crystallization at higher temperatures, and so a larger crystal thickness can be observed. In addition, the existing crystallites might undergo perfectioning and probably some melting of the less stable crystallites processes which are finally followed by a complete recrystallization. Interesting to note is that the melting−recrystallization processes found up to $T_c = 220$ °C did not occur just once, but it proceeded in a repetitive manner at increasing temperature, leading all samples to a common final melting temperature of 232 °C. This is expected as the final melting temperature of the recrystallized crystallites depends only on the effective heating rate of the experiment, which was about 0.2 °C/min for all the SAXS heating experiments.

Now we turn to address the problem of constructing the G−T melting line for all samples of the three ranges. This was a straightforward process in the first range, as T_f there can be readily determined. The same was true in the second range; here T_f was taken as the temperature at which the crystal thickness started to increase during heating. In the third range, the situation was more complicated as more than one effect are involved here, as indicated earlier, and an accurate determination of the melting point was unattainable. Therefore, we have constructed the melting line based upon the results of the first and the second ranges only. On the other hand, the crystallization line was constructed by including the results of all three ranges. Figure 3 shows the resulting melting line and the crystallization line together with the changes of the reciprocal of the crystal thickness with temperature during heating. It can be seen that the samples in the second range followed the melting line during their recrystallization at high temperatures. The samples in the third range also eventually followed the melting line at higher temperatures. This indicates that the recrystallized crystallites and any other newly formed crystallites during heating melt at the same melting line. It is also evident that the melting line intersected the crystallization line at a finite crystal thickness and not at $d_c^{-1} = 0$. The temperature at which the intersection occurred was about 243 °C. This value falls very close to the values reported by several authors for the equilibrium melting temperature of iPS of a similar stereoregularity using the H−W extrapolative method, namely 242 °C.[24,25]

The melting line of Figure 3 can be expressed as

$$T_f = T_f^\infty - C_1 d_c^{-1} \tag{6}$$

where T_f is the observed melting temperature, T_f^∞ is the intercept which also represents the equilibrium melting temperature, and C_1 is the gradient. A linear regression of the melting line to such an equation resulted in a value of 289 °C for T_f^∞. As we have some data scatter of unknown origin, this is not a sharp value but has an uncertainty of about ±5 °C. One can appreciate the large difference between the commonly reported value and our new value. In fact, doubts about the reported value of T_f^∞ of iPS obtained by the H−W method were raised first back in 1972 in the work of Lemstra et al.[25] They measured melting temperatures which were some degrees higher than 242 °C for samples prepared by the self-seeding technique. Recently, Lieberwirth and Petermann[26] have measured an even higher melting temperature, of 255 °C, for iPS samples with a shish kebab morphology prepared using the injection molding technique.

In a similar manner the crystallization line of Figure 3 can be written as

$$T_c = T_c^\infty - C_2 d_c^{-1} \tag{7}$$

where T_c^∞ is the intercept and C_2 is the gradient. The existence of such a line is the common result of the time-dependent SAXS studies of the isothermal crystallization of all the semicrystalline polymers that we have studied. Because it is always different from the melting line, we understand it as the thickness dependence of a phase transition different from that described by the melting line. We have tentatively related it to a transition from a mesomorphic to a granular crystalline phase which takes place along a multistep route followed by polymers in their transition from an entangled melt to a semicrystalline state.[18]

Normally, the G−T melting line is constructed on the basis of DSC measurements and not on SAXS measurements. Therefore, it is of interest to compare the SAXS melting line with that obtained from DSC measurements, in particular for samples that show the melting recrystallization phenomenon. For this purpose, we recorded the DSC melting curves for samples isothermally cold crystallized at different crystallization temperatures, and the results, obtained at a heating rate of 0.5 °C/min, are presented in Figure 4. As can be seen, two or three melting endotherms were observed depending on the crystallization temperature. This is a typical behavior for samples that show recrystallization after melting during the heating scan and has been

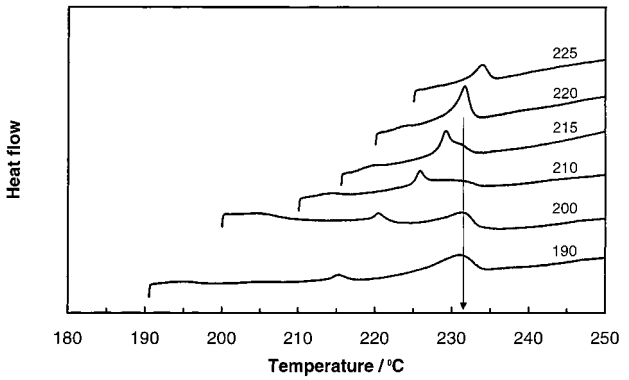

Figure 4. DSC melting curves of samples crystallized at the indicated crystallization temperatures, obtained at a heating rate of 0.5 °C/min.

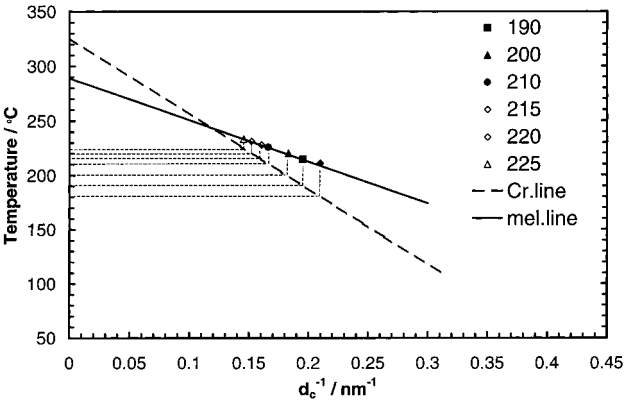

Figure 5. Comparison between the melting lines obtained from the temperature-dependent SAXS measurements and the DSC measurements.

observed by several workers. We just state here their main findings regarding the origin of these different endotherms. The minor endotherm, sometimes addressed as the annealing peak, always lies at 5−10 °C above T_c and has been associated with the melting of small crystallites coupled to the mobilization of a rigid amorphous third phase.[27,28] The low-temperature melting endotherm corresponds to the melting of the initial crystallites formed at the crystallization temperature, and the high-temperature endotherm is attributed to the melting of the crystallites formed by recrystallization after melting of the initial lamellae during the heating scan.[25] As can be seen, the position of the high-temperature endotherm remained independent of the crystallization temperature at 231.7 °C, which agrees with the final melting temperature observed by the SAXS measurements. The low-temperature endotherm varied with the crystallization temperature. Therefore, only the low endotherm should be used in constructing the G−T melting line. The low endotherm values of Figure 4 are plotted on the same graph which shows also the SAXS melting and crystallization lines of Figure 3, in Figure 5. One can see that there is a good match between the DSC melting temperatures and the SAXS melting line, particularly at high temperatures where a perfect agreement is evident. As the crystallization temperature decreases, a minor discrepancy between the DSC values and melting line arises, reaching a value of about 2 °C at a crystallization temperature of 180 °C.

4. Conclusions

The Gibbs−Thomson melting line was used to determine the equilibrium melting temperature of iPS. This line was constructed on the basis of temperature-dependent SAXS measurements which allowed the opportunity to record the crystal thickness and the melting temperature of the same lamellae. A new value of 289 ± 5 °C was found, which is much higher than the commonly reported values obtained by the Hoffman−Weeks extrapolative method, namely 242 °C.

This study proves that even for polymers that undergo recrystallization during heating, the Gibbs−Thomson melting line as obtained by the temperature-dependent SAXS measurements can be used to determine T_f^{∞}.

Acknowledgment. We thank the Graduiertenkolleg "Strukturbildung in Makromolekularen Systemen" for the financial support of M. Al-Hussein.

References and Notes

(1) Hoffman, J. D.; Davis, G. T.; Lauritzen, J. I. In *Treatise on Solid State Chemistry*; Plenum: New York, 1976; Vol. 3, p 497.
(2) Hoffman, J. D.; Miller, R. L. *Polymer* **1997**, *38*, 3151.
(3) Strobl, G. *The Physics of Polymers*; Springer: Berlin 1996.
(4) Wunderlich, B. *Macromolecular Physics*; Academic Press: New York, 1980; Vol. 3.
(5) Hoffman, J. D.; Weeks, J. J. *J. Res. Natl. Bur. Stand. (U.S.)* **1962**, *A66*, 13.
(6) Schmidtke, J.; Strobl, G.; Thurn-Albrecht, T. *Macromolecules* **1997**, *30*, 5804.
(7) Hauser, G.; Schmidtke, J.; Strobl, G. *Macromolecules* **1998**, *31*, 6250.
(8) Heck, B.; Hugel, T.; Iijima, M.; Sadiku, E.; Strobl, G. *New J. Phys.* **1999**, *1*, 17.
(9) Iijima, M.; Strobl, G. *Macromolecules* **2000**, *33*, 5204.
(10) Fu, Q.; Heck, B.; Strobl, G.; Thomann, Y. *Macromolecules* **2001**, *34*, 2502.
(11) Marand, H.; Xu, J.; Srinivas, S. *Macromolecules* **1998**, *31*, 8219.
(12) Kanig, G. *Colloid Polym. Sci.* **1991**, *269*, 1118.
(13) Tashiro, K.; Sasaki, S.; Gose, N.; Kobayashi, M. *Polym. J.***1998**, *30*, 485.
(14) Pogodina, N. V.; Siddiquee, S. K.; van Egmond, J. W.; Winter, H. H. *Macromolecules* **1999**, *32*, 1167.
(15) Hobbs, J. K.; McMaster, T. J.; Miles, M. J.; Barham, P. J. *Polymer* **1998**, *39*, 2437.
(16) Hobbs, J. K.; Humphries, A. D. L.; Miles, M. J. *Macromolecules* **2001**, *34*, 5508.
(17) Ezure, H.; Kimura, T.; Ogawa, S.; Ito, E. *Macromolecules* **1997**, *30*, 3600.
(18) Strobl, G. *Eur. Phys. J. E* **2001**, *3*, 165.
(19) Strobl, G. *Acta Crystallogr.* **1970**, *26A*, 367.
(20) Ruland, W. *Colloid Polym. Sci.* **1977**, *255*, 417.
(21) Brandrup, J., Immergut, E. H., Eds. *Polymer Handbook*; Wiley: New York, 1979.
(22) Petermann, J.; Gohil, R. M. *Prog. Colloid Polym. Sci.* **1979**, *66*, 41.
(23) Liu, T.; Petermann, J.; He C.; Liu, Z.; Chung, T. S. *Macromolecules* **2001**, *34*, 4305.
(24) Boon, J.; Challa, G.; Van Krevelen, D. W. *J. Polym. Sci., Polym. Phys. Ed.* **1968**, *6*, 1791.
(25) Lemstra, P. J.; Kooistra, T.; Challa, G. J. *J. Polym. Sci., Part A-2* **1972**, *10*, 823.
(26) Liu, T. X.; Lieberwirth, I.; Petermann, J. *J. Macromol. Chem., Phys.*, in press.
(27) Lu, S. X.; Cebe, P. *Macromolecules* **1997**, *30*, 6243.
(28) Schick, C.; Wurm, A.; Mohamed, A. *Colloid Polym. Sci.* **2001**, *279*, 800.

MA011345K